



ELSEVIER

Physica B 241–243 (1998) 64–70

PHYSICA B

## Backscattering spectroscopy at the NIST Center for Neutron Research

P.M. Gehring\*, D.A. Neumann

*NIST Center for Neutron Research, National Institute of Standards and Technology, Gaithersburg, MD 20899, USA*

### Abstract

We discuss the design of a new backscattering spectrometer that is soon to become operational at the NIST Center for Neutron Research. Both monochromator and analyzer are composed of spherically bent Si (1 1 1) crystals that focus the incident and scattered neutron beams. The bending increases the intrinsic lattice gradient of Si beyond its Darwin limit, resulting in an energy resolution of about 0.75  $\mu\text{eV}$  FWHM. The Doppler-driven monochromator should provide a wide dynamic range of  $\pm 50 \mu\text{eV}$ . The elastic  $Q$ -range will cover 0.15–1.8  $\text{\AA}^{-1}$ . The most novel component of this spectrometer is the phase-space-transform chopper. This device rotates at 4730 rpm while neutrons are Bragg-diffracted from sets of HOPG crystals affixed to its periphery. The process enhances the neutron flux at the backscattered energy of 2.08 meV, but at the expense of a larger horizontal divergence. This effectively reduces the divergence mismatch between primary and secondary spectrometers, a long standing problem with backscattering instruments. Simulations suggest a resultant flux increase of order 3 should be obtained. © 1998 Elsevier Science B.V. All rights reserved.

*Keywords:* Neutron scattering; Backscattering; Instrumentation; Phase space transformation; Inelastic; Quasielastic

### 1. Introduction to backscattering

Neutron backscattering spectroscopy was first proposed in 1966 by Maier-Leibnitz [1,2]. The technique exploits the fact that the wavelength spread  $\Delta\lambda$  of a Bragg-reflected neutron beam becomes increasingly narrow as the scattering angle  $2\theta$  approaches  $180^\circ$ , hence the term backscattering. This can be shown most simply by differentiating Bragg's law and dividing the result by  $\lambda$  to obtain

$$\frac{\Delta\lambda}{\lambda} = \frac{\Delta d}{d} + \frac{\Delta\theta}{\tan\theta} \quad (1)$$

\*Corresponding author. Fax: (301) 921-9847; e-mail: peter.gehring@nist.gov.

As  $\theta \rightarrow 90^\circ$  the angular term vanishes. This results in a minimum in  $\Delta\lambda/\lambda$ , and thus the energy resolution, that depends on the spread  $\Delta d$  and average value  $d$  of the lattice spacing between Bragg planes. In the kinematic limit this minimum is zero. However, dynamical scattering theory shows that the lattice gradient term  $\Delta d/d$  is finite, even for perfect single crystals. In this case,  $\Delta d/d$  is given by the Darwin width of the reflection being used to monochromate the neutron beam. Hence there is a fundamental lower bound to the energy resolution that can be obtained via backscattering. This bound depends entirely on the structure factor of the reflection and the number density of unit cells.

Neutron beams are never perfectly collimated. Hence some neutrons are incident at angles slightly less than or slightly greater than  $\theta = 90^\circ$  and will satisfy the Bragg condition at different values of  $\lambda$ . Thus the beam divergence also contributes to  $\Delta\lambda$  [3]. For simplicity the lattice and divergence terms can be added linearly so that, for small  $\Delta\theta$ ,

$$\frac{\Delta E}{E} = 2 \frac{\Delta\lambda}{\lambda} = 2 \left( \frac{\Delta d}{d} + \frac{1}{8}(\Delta\theta)^2 \right), \quad (2)$$

where  $\Delta\theta$  represents the incident beam divergence. Most backscattering instruments use the  $\{111\}$  lattice planes of perfect silicon as monochromator and analyzer. For this case,  $\Delta d/d = 1.86 \times 10^{-5}$ ,  $\lambda = 2d = 6.271 \text{ \AA}$ , and  $E = 2.08 \text{ meV}$ . A matching divergence term of only  $0.70^\circ$  in Eq. (2) gives an energy resolution of order  $0.16 \text{ } \mu\text{eV}$ . Obviously the price one pays for such a narrow energy resolution is low neutron flux on the sample. This limits the practical use of backscattering spectrometers to high-flux reactors and to studies of samples which are strong neutron scatterers.

## 2. The high-flux backscattering spectrometer

In an effort to increase the sample flux, we have incorporated state-of-the-art neutron optics into the design of a “high-flux” backscattering spectrometer (HFBS), which is to be installed on guide NG-2 at the National Institute of Standards and Technology Center for Neutron Research [4]. The primary goal of our design is to maximize the incident flux while keeping the instrumental energy resolution below  $1 \text{ } \mu\text{eV}$ . In this respect the HFBS can be considered as a complement to the higher resolution backscattering spectrometers located at the ILL, Grenoble, France, and KFA, Jülich, Germany.

We discuss the various components of the HFBS below in order from reactor to detectors. Where appropriate we report on the performance of specific parts of the instrument (e.g. the converging guide) based on preliminary measurements.

### 2.1. The primary spectrometer

The primary spectrometer consists of the NG-2 guide system, the converging guide, the phase-space

transform (PST) chopper, and the monochromator as shown in Fig. 1 (analyzer and detectors are not shown). The NG-2 guide is a straight guide that views a liquid hydrogen cold source with an effective Maxwellian temperature of 45 K. The neutron source flux at  $6.2711 \text{ \AA}$  is estimated to be  $\sim 1.5 \times 10^{11} \text{ n/(cm}^2 \text{ s Sr \AA)}$ . Neutrons are conducted from the cold source to the HFBS along a guide that is 15 cm high by 6 cm wide. The top and bottom interior surfaces of this guide are coated with NiCTi supermirrors ( $Q_c = 0.044 \text{ \AA}^{-1}$ ), whereas the sides are coated with  $^{58}\text{Ni}$ -equivalent supermirrors ( $Q_c = 0.026 \text{ \AA}^{-1}$ ) [5].

Be and Bi filters, positioned far upstream from the HFBS, remove fast neutrons and gamma radiation from the beam. At present we have installed 10 cm of each, with provision for an additional 20 cm of filter material. A neutron velocity selector, placed just after the two filters, is used to limit  $\Delta\lambda/\lambda$  to 18% in order to minimize the background arising from neutrons whose wavelength lies outside the bandwidth accepted by the HFBS. The blades of the velocity selector are 0.4 mm thick carbon fibre in epoxy loaded with  $^{10}\text{B}$  as absorber material. This gives a relative suppression of unwanted neutrons of  $2 \times 10^{-4}$ , and a peak transmission of 83%.

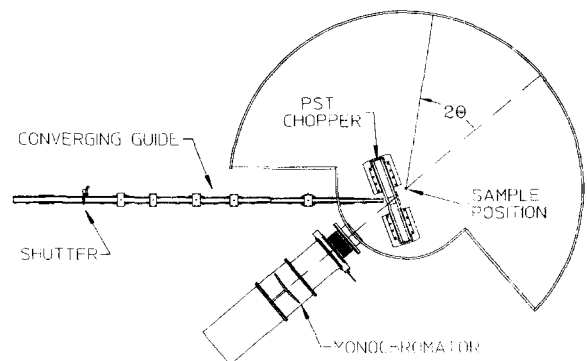


Fig. 1. This simplified schematic diagram shows the primary spectrometer layout for the HFBS. After the NG-2 straight guide, the converging guide begins to focus the 15 cm by 6 cm beam cross section down to  $2.8 \times 2.8 \text{ cm}$  over a distance of 4 m. Next the PST chopper deflects the neutrons into the monochromator where they are backscattered onto the sample position.

## 2.2. The converging guide

The converging guide section on NG-2 begins approximately 48 m downstream from the cold source. All four of its interior surfaces are coated with  $2\theta_c^{\text{Ni}}$  supermirrors. It focusses the NG-2 beam cross section down to 2.8 cm square. The focussing in the vertical takes place over 4 m, while the focussing in the horizontal begins 1 m further downstream, and takes place over 3 m. Assuming a uniform illumination of the entrance of the converging guide, and perfect reflectivity of the supermirror coatings out to the critical angle, the flux at the exit of the guide should be 3.10 times greater than that at the entrance. More detailed Monte Carlo simulations show that this flux enhancement factor increases to 3.33 when one takes into account the substantial 87 cm guide cut 13.5 m upstream where the Be/Bi filter and neutron velocity selectors are situated, and when one uses a realistic reflectivity profile for the supermirror coatings. The reason the enhancement increases is that the more highly divergent neutrons are preferentially lost in the guide cut, and thus are not present at the entrance to the converging guide. These are also the first neutrons to be lost in the converging guide, thereby making the enhancement larger.

Two sets of measurements were made to characterize the performance of the converging guide. Gold foil activation measurements indicated a thermal capture flux of  $2.15 \times 10^8$  n/cm<sup>2</sup>/s at the entrance to the converging guide just before the shutter, and a thermal capture flux ( $\sigma_{\text{abs}} = 98.65$  barns at 1.8 Å) of  $8.29 \times 10^8$  n/cm<sup>2</sup>/s at the exit of the guide. This corresponds to a flux gain of 3.89 for the guide, about 17% higher than expected from the Monte Carlo simulations. It is possible to explain this difference by simply postulating a slightly higher critical angle for the supermirror coatings in the converging guide, or by reducing the reflectivity of those in the straight guide near the critical angle. But without a precise measurement of the reflectivity profiles of the supermirror coatings used in the straight and converging guides, it is not possible to obtain better agreement between simulations and measurements.

In addition to the gold foil measurements, we also took autoradiograph images of the beam

before and after the converging guide by irradiating two separate 125 μm thick Dy foils. Irradiation times were 64 s in each case (performed separately). The autoradiograph images were used to detect evidence of “stripes” in the beam profile due to the guide cut. None were evident. However any stripes would likely be “washed out” by the bandwidth of the velocity selector. The integrated intensities over five independent 14 mm<sup>2</sup> circular regions were calculated from which it was determined that the total beam intensity does not vary more than 8% over the exit of the converging guide. When integrated over the entire beam these measurements indicate a flux gain of 3.43 for the converging guide.

## 2.3. The phase space transformation chopper

The function of the PST chopper is to transform the shape of the incoming neutron beam in phase space such that the neutron flux of the diffracted beam is enhanced at the backscattering energy  $E_0 = 2.08$  meV. This idea, due to Schelten and Alefeld [6], was developed to address the significant mismatch in divergence between primary and secondary spectrometers. To our knowledge, the HFBS is the first instrument to incorporate a PST chopper into its design.

The HFBS PST chopper consists of a disk of diameter 1 m whose periphery is divided into six sectors. Alternate sectors are covered with HOPG crystals 3.5 cm high which are mounted inside cassettes. The mosaic spread of an individual HOPG crystal was chosen to be 2.5° FWHM. Three crystals are then stacked between spacers inside the cassettes to give an effective horizontal mosaic spread of roughly 7.5°.

As shown in the leftmost panel of Fig. 2, with the chopper at rest, the incoming beam has a relatively small angular divergence that is set by the critical angle for internal reflection of the guide wall coatings, but a significant spread in wavevector  $\Delta k$  ( $k = 2\pi/\lambda$ ). After diffracting from an HOPG crystal having a mosaic spread of 5° FWHM, the outgoing phase space element has a much broader divergence. The middle panel demonstrates what happens when the HOPG crystals are rotated parallel to  $-\mathbf{k}_x$  at a linear speed of 250 m/s. The

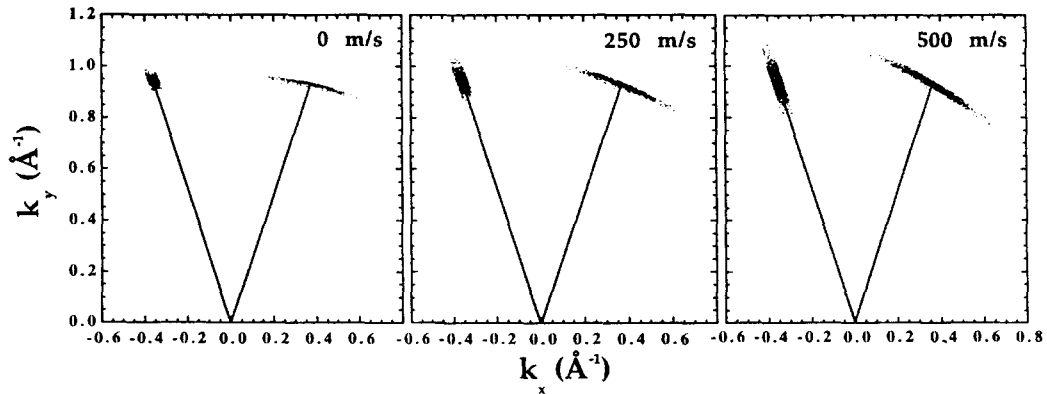


Fig. 2. Simulations of Bragg diffraction from PG crystals with an intrinsic mosaic spread of  $5^\circ$  FWHM, moving at three different speeds. The simulations have been projected from 3-D onto the  $(k_x, k_y)$  plane.

outgoing phase space element is now both larger and more divergent, and it is tilted such that its arc is essentially perpendicular to  $k_f$ . This tilt produces a much narrower energy spread about  $E_0$ , thereby increasing the neutron flux at the desired backscattering energy of 2.08 meV. Increasing the chopper speed to 500 m/s as shown in the rightmost panel results in an even more pronounced tilt. In this case, however, the tilt is too large so that the effective flux enhancement at  $E_0$  not optimal.

The mosaic spread of  $7.5^\circ$  was chosen on the basis of detailed computer simulations of the PST chopper over a range of mosaic spreads and chopper speeds. The results are summarized in Fig. 3 and will be discussed in greater length in a future publication that will also include experimental measurements of the PST chopper gain factor [7].

#### 2.4. The monochromator system

The HFBS monochromator is 52 cm wide by 28 cm tall, and is spherically curved to a radius of 2.12 m in order to focus the neutrons diffracted by the PST chopper onto the sample position which is 2.25 m from the monochromator. The larger width is required to capture most of the neutrons scattered from the PST chopper which greatly increases the horizontal divergence of the scattered beam from  $3^\circ$  to over  $17^\circ$ .

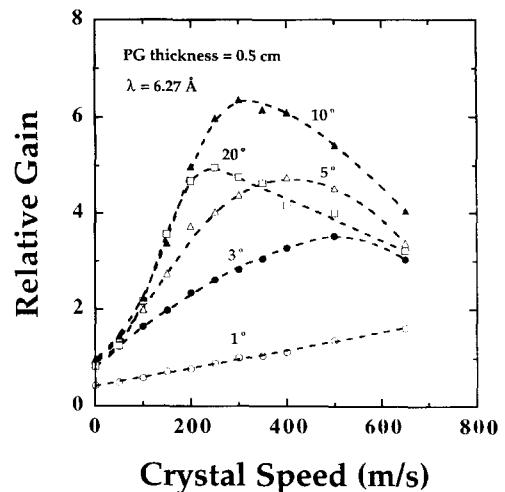


Fig. 3. Peak intensity relative to that for a stationary chopper.

In order to maintain the backscattering condition, and hence the high energy resolution, the incident neutron energy  $E_i$  is varied via Doppler motion of the monochromator along the neutron beam direction. The backscattered neutrons then pass through the rotating PST chopper (which during this time has rotated out of the path of the scattered beam) and scatter from the sample.

Many authors have discussed Bragg diffraction from moving lattices in detail [8,9]. Backscattering from a moving monochromator is a special case of this for which the neutron velocity is parallel to the

motion of the crystal. In this case, the energy shift of backscattered neutrons relative to  $E_0$  is given by

$$\Delta E = E_m - E_0 = 2E_0 \left( \frac{v_m}{v_0} \right) + E_0 \left( \frac{v_m}{v_0} \right)^2, \quad (3)$$

where  $v_m$  is the velocity of the monochromator, and  $v_0 = 630.8 \text{ m/s}$  for  $6.271 \text{ \AA}$  neutrons. It is important to bear in mind that the energy bandwidth diffracted by the PST is roughly  $100 \mu\text{eV}$  FWHM. This effectively limits the dynamic range of the instrument.

The Doppler drive has a top frequency of 25 Hz and an amplitude of  $\pm 4.5 \text{ cm}$ , corresponding to a peak energy transfer of  $\pm 50 \mu\text{eV}$ . The drive mechanism, shown in Fig. 4, employs a cam machined to give a velocity profile best described as a rounded triangular waveform. This profile avoids the abrupt change in the acceleration that would occur with a purely triangular waveform. The linear portions of the velocity profile are desirable because they weight all energy transfers equally. A sinusoidal waveform, by contrast, spends more time at the maximum speeds, thereby weighting higher energy transfers more heavily. A second cam

with a sinusoidal profile will also be available for use on the HFBS.

A measurement of the velocity profile was made recently using a laser vibrometer that provides an analog output directly proportional to the instantaneous velocity of the monochromator. The profile, shown in Fig. 5, corresponds to  $3 \text{ m/s}$ , or  $\sim \pm 20 \mu\text{eV}$  energy transfer. Some “ripples” are clearly evident on various portions of the waveform, and these are not well understood at present. Tests of the Doppler drive system are still in progress.

### 2.5. The secondary spectrometer

Backscattering instruments must have large, spherically focussed analyzers that cover as much solid angle as possible in order to compensate for the inherently low neutron flux on the sample. The HFBS analyzer stands  $2 \text{ m}$  tall, spans  $165^\circ$  in  $2\theta$ , and subtends 20% of  $4\pi$  steradians. The analyzer is spherically curved to a radius of  $2.05 \text{ m}$  in order to focus the backscattered neutrons onto the detectors (not the sample). An important gain in flux

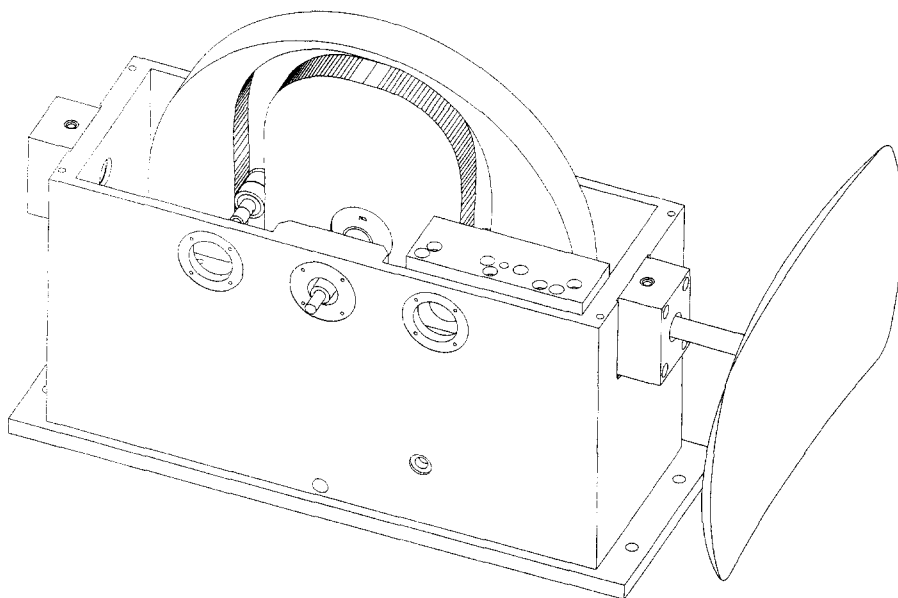


Fig. 4. Schematic diagram of the Doppler drive system.

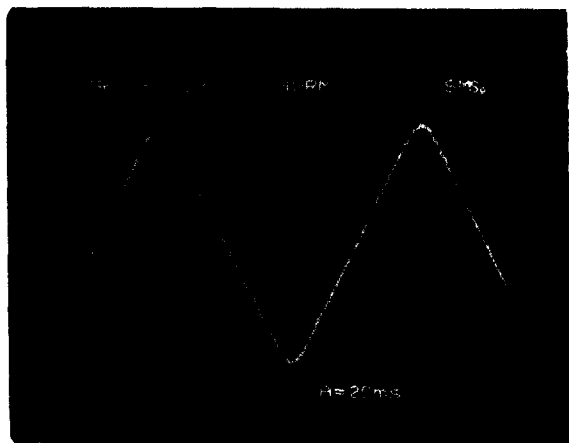


Fig. 5. Velocity profile of the HFBS Doppler drive at 3 m/s, which corresponds to an energy transfer of  $\pm 20 \mu\text{eV}$ . The measurements were made using a laser vibrometer.

is obtained by gluing large diameter ( $\sim 125 \text{ mm}$ ) Si(111) wafers onto both the analyzer and monochromator backing plates. The bending increases the intrinsic lattice gradient of Si beyond its Darwin limit, resulting in a higher flux at the expense of an increased instrumental energy resolution.

The amount by which  $\Delta d/d$  changes with bending depends on both the radius of curvature  $R_c$  and the crystal wafer thickness  $t$  according to the expression

$$\frac{\Delta d}{d} = \left(\frac{\Delta d}{d}\right)_{\text{Darwin}} + P_{\text{eff}} \left(\frac{t}{R_c}\right), \quad (4)$$

where  $P_{\text{eff}}$  is an effective Poisson's ratio which, for spherically bent Si(111), is about 0.44 [10].

The preceding equation predicts that a thickness of only  $150 \mu\text{m}$  is sufficient to obtain an energy resolution of order  $0.75 \mu\text{eV}$  FWHM. Two sets of extensive tests were carried out at the ILL on IN16 using small analyzer prototypes with Si(111) thicknesses from  $250$  to  $950 \mu\text{m}$  in order to determine the optimal wafer thickness experimentally. The results of these measurements were surprising as they indicated a much weaker dependence of the energy resolution on the wafer thickness  $t$ . Moreover, it was observed that Si(111) thicknesses less than  $700 \mu\text{m}$  did not fully saturate the reflectivity.

Based on these results a value of  $700 \mu\text{m}$  was chosen for the thickness of the Si(111) wafers covering the monochromator and analyzer. In addition, it was found that chemically etching the wafers resulted in a nearly perfect Gaussian form to the resolution function, whereas the resolution function measured with unetched wafers had a strong Lorentzian component.

### 3. Estimated instrumental characteristics

The Au foil activation measurements indicate that the neutron flux at  $6.271 \text{ \AA}$  at the exit of the converging guide is  $2.4 \times 10^8 \text{ n/cm}^2/\text{s}$ . Assuming a moderate gain factor of only 3 for the PST chopper, and reasonable reflectivities from the HOPG and Si(111), this corresponds to a flux at the sample position of about  $2 \times 10^5 \text{ n/cm}^2/\text{s}$ . The target instrumental energy resolution for the NIST HFBS is  $0.75 \mu\text{eV}$  FWHM. Based on the tests on IN16 we expect to be within 20% of this goal.

With the HFBS Doppler drive running at top speed, users will have access to a dynamic range of  $-50 \mu\text{eV} \leq \Delta E \leq +50 \mu\text{eV}$ . This is fully twice the dynamic range available at either IN10 or IN16 at a comparable energy resolution [11]. An extension of the HFBS dynamic range, as well as that of IN10 and IN16, is foreseen through the use of  $\text{Si}_{1-x}\text{Ge}_x$  single crystals as alternate monochromators. These alloys have slightly larger lattice spacings compared to pure Si, and shifts of the elastic line corresponding to  $15 \mu\text{eV}$  have already been measured by Magerl and Holm using single crystals of  $\text{Si}_{0.9}\text{Ge}_{0.1}$  [12]. It should be reiterated, however, that one cannot extend the dynamic range indefinitely since the energy bandwidth diffracted by the PST is finite. A significant reduction in intensity can be expected at energy transfers beyond  $\sim 50 \mu\text{eV}$ , making the high-flux design of the HFBS all the more important.

### Acknowledgements

We wish to acknowledge Dick Lindstrom and Tony Cheng who performed the Au and Dy foil

irradiation measurements, respectively. In addition we would also like to thank Bernhard Frick for his help and invaluable assistance with the tests on IN16 which were used to determine the optimal Si(1 1 1) wafer thickness for the analyzer and monochromator. Finally, the authors would like to acknowledge the hospitality of Brookhaven National Laboratory where extensive use was made of the High Flux Beam Reactor during tests of the many hundreds of HOPG crystals that were required to construct the PST chopper.

## References

- [1] H. Maier-Leibnitz, *Nukleonik* 8 (1966) 61.
- [2] B. Alefeld, Bayer, Akademie der Wissenschaften, Math. Naturwiss. Klasse 11 (1966) 109.
- [3] M. Birr, A. Heidemann, B. Alefeld, *Nucl. Instr. and Meth.* 95 (1971) 435.
- [4] D.A. Neumann, B. Hammouda, *J. Res. Nat. Inst. Stand. Tech.* 98 (1993) 89.
- [5] C.F. Majkrzak, J.F. Ankner, in: C.F. Majkrzak, J.L. Wood, (Eds.), *Neutron Optical Devices and Applications*, SPIE Proc. Vol. 1738, SPIE, Bellingham, WA, 1992, p. 150.
- [6] J. Schelten, B. Alefeld, in: R. Scherm, H.H. Stiller (Eds.), *Proc. Workshop on Neutron Scattering Instrumentation for SNQ*, Report Jül-1954 1984.
- [7] D.A. Neumann, P.M. Gehring, C.W. Brocker, to be published.
- [8] C.G. Shull, N.S. Gingrich, *J. Appl. Phys.* 35 (1964) 678.
- [9] B. Buras, T. Giebultowicz, *Acta. Crystallogr. A* 28 (1972) 151.
- [10] A.D. Stoica, M. Popovici, *J. Appl. Crystallogr.* 22 (1989) 448.
- [11] *Guide to Neutron Research Facilities at the ILL*, 1994, p. 108.
- [12] A. Magerl, C. Holm, *Nucl. Instr. and Meth. A* 290 (1990) 414.